ATR-77(7523-30)-3

[redacted]

THE AEROSPACE CORPORATION
El Segundo, California 90245

1.3

Aerospace Report No.
ATR-77(7523-20)-3

ATMOSPHERIC ATTENUATION OF SOLAR RADIATION

18 May 1977

Prepared by

THE AEROSPACE CORPORATION
Energy Systems Group
El Segundo, California 90245

Principal Contributor:

C. M. Randall, Chemistry and Physics Laboratory

FOREWORD

This report is written as a partial account of work performed for the Energy Research and Development Administration, on the Central Receiver Program, under continuation of Contract Number EY76-C-03-1101.

ABSTRACT AND SUMMARY

The attenuation of solar radiation by the atmosphere between the heliostat and receiver of a Central Receiver solar energy system has been computed for a number of atmospheric conditions and tower-heliostat distances. The most important atmospheric variable is found to be the atmospheric aerosol content. No dependence of atmospheric water vapor is found and only a weak dependence on solar zenith angle. For a 500 m heliostat-tower distance two to four percent reductions are expected under typical desert conditions (50 to 120 km visibility). The reduction is approximately linear with heliostat-tower distance. A representative value of the attenuation coefficient is 0.051 km^{-1}.

REDUCTION OF INSOLATION IN A CENTRAL RECEIVER SYSTEM FOR VARIOUS METEOROLOGICAL CONDITIONS

I. INTRODUCTION

The transfer of solar radiation into the receiver of a Central Receiver concept solar energy system requires the transmission of the radiant energy through an atmospheric path between the heliostat and the receiver which may be several hundred meters long. The calculations reported here indicate that there is an attenuation of radiation along this path which may be appreciable under some atmospheric conditions. This implies that there is an atmospheric loss term for these applications in addition to that automatically included in the usually available insolation measurement. The procedures used to make the calculations reported here are similar to those used in Ref. 1 to evaluate the atmospheric spectral attenuation effects on solar cell performance.

II. FORMULATION

The total radiant energy available at the surface of a receiver in a solar energy system is proportional to E, where

$$E = (\Delta\nu)^{-1} \int_{\Delta\nu} T(\nu)R(\nu)H(\nu)d\nu. \qquad (1)$$

$T(\nu)$ is the atmospheric transmittance at frequency ν, $R(\nu)$ is the transmittance of any optical windows in the path of the radiation and $H(\nu)$ is the solar irradiance at frequency ν. We choose $R(\nu)$ to characterize Pyrex glass, which has a flat response over most of the solar spectrum and to make the results computed here easily comparable with customarily observed insolation measurements.

The integral in Equation (1) is expressed in terms of frequency, ν, measured in wavenumbers rather than wavelength, $\lambda = 1/\nu$ measured in microns, because the atmospheric transmittance program, LOWTA, provides the capability of computing E in wavenumber space, but not wavelength space. The standard solar spectral irradiance spectrum, Table 1,

on the other hand, is available in wavelength units (Ref. 2). To convert it is necessary to multiply by $|d\lambda/d\nu| = \lambda^2 = \nu^{-2}$. Table 2 contains the solar spectrum in units of wavelength at evenly spaced increments of ν as determined by visual interpolations of a plot of the spectrum tabulated in Table 1.

Employing units of the quantity tabulated in Table 2, Equation 1 becomes

$$E = (\Delta\nu)^{-1} \int_{\Delta\nu} T(\nu)[R(\nu)H_\lambda(\nu)/\nu^2]d\nu \tag{2}$$

Since only relative responses are required, this expression can be scaled by the peak value of the quantity in brackets, $\rho = [R(\nu)H_\lambda(\nu)/\nu^2]$.

$$E = \rho(\Delta\nu)^{-1} \int_{\Delta\nu} T(\nu)r(\nu)d\nu = \rho I \tag{3}$$

where

$$r(\nu) \equiv [R(\nu)H_\lambda(\nu)/\nu^2]/\rho \tag{4}$$

If E_0 is proportional to energy received by a pyrheliometer at the surface of the earth, and E_p is proportional to the energy after traversing an additional atmospheric path, then y is the fractional additional reduction in energy caused by the extra path length.

$$y = (E_0 - E_p)/E_0 = 1 - E_p/E_0 \tag{5}$$

$$= 1 - I_p/I_0 \tag{6}$$

The computations of I were carried out with computer program LOWTA (Ref. 3), based on the Air Force Geophysics Laboratory code LOWTRAN3 (Ref. 4). The input to LOWTA is a specification of the

atmospheric model, the path through the atmosphere, the response function, $r(\nu)$ and the limits of integration. The transmittance of pyrex, R, used is shown in Table 3 and the resulting normalized response function, r, is shown in Table 4.

III. ATMOSPHERIC MODELS

The major variable atmospheric constituents affecting the solar radiation are aerosols and water vapor. Variations in water vapor have been studied parametrically by making calculations for three different vertical profiles of atmospheric constituents. As far as solar transmittance is concerned, these model atmospheres differ principally in their water content. The tropical model contains 5.15gm cm^{-2} in a vertical path from space to the earth's surface. By comparison the midlatitude-summer model contains 3.68gm cm^{-2} and the midlatitude winter model 1.05gm cm^{-2}. The quantitative specification of these atmospheres is contained in Reference 3 and based on Air Force Geophysics Laboratory models (Ref. 5).

Aerosols are the most important attenuation mechanism in the present problem and so attenuation modeling for this constituent is dealt with in detail. The LOWTA/LOWTRAN3 aerosol attenuation model is basically a single scattering model, which is applicable up to attenuations of 50 to 60 percent. The percent study involves attenuations of 20 percent or less, thus this simplified approach is applicable. In the single scattering approximation the aerosol transmittance factor, $t(\nu)$, of an atmospheric path depends exponentially on an integration along the atmospheric path, x.

$$t(\nu) = \exp\left[-\int_{x} N(x)B(x,\nu)dx\right] \tag{7}$$

$N(x)$ is the number density of particles at position x along the path. $B(x,\nu)$ is extinction coefficient and will in general depend on both path position

and frequency, ν. Aerosols occur with a wide range of radius, r, so the computations of B at any path position requires an integration over particle size.

$$B(x, \nu) = \int_r f(r, x)\sigma(x, r, \nu)dr \tag{8}$$

$f(r,x)$ is the size distribution normalized so that $N(x)f(r,x)$ is the actual numerical size distribution at positions x. $\sigma(x, r, \nu)$ is the extinction cross section at frequency ν for a particle of size r. This is dependent on path position, x, only if the chemical composition of the particles, and thus their refractive indices, varies along the path. The mathematical problem is usually made tractable by assuming the aerosol particles are spherical and composed of a material of known complex refractive index. The cross section σ can be computed by means of Mie theory. Within the LOWTA and LOWTRAN3 programs used in this study both the composition and normalized size distribution, f, are assumed to be independent of path position so that B becomes independent of path.

$$B(\nu) = \int_r f(r)\sigma(r, \nu)dr \tag{9}$$

The empirical observation of aerosol attenuation cannot by itself separate the effects of changes in B and N(x). Therefore, it is customary to discuss experiments simply in terms of the aerosol attenuation coefficient, $\beta(x)$.

$$t(\nu) = \exp[-\int_x \beta(x, \nu)dx] \tag{10}$$

$$\beta(x, \nu) = N(x)B(x, \nu) \tag{11}$$

Within the approximations used in the LOWTA/LOWTRAN3 programs,

$$\beta(x, \nu) = N(x)B(\nu), \tag{12}$$

thus a specification of $\beta(x, \nu)$ at any frequency can be used to specify $N(x)$ and used in the program to compute transmittance at other frequencies.

In the visible portion of the spectrum where the principal aerosol attenuation mechanism is scattering and not absorption the "meteorological range", "visual range", or "visibility", D_m can be quantitatively related to the aerosol attenuation coefficient, β, under the following assumptions:

- The scattering and attenuation coefficients are the same, i.e., there is no aerosol absorption.
- The minimum radiance difference the eye can detect is two percent.
- The visibility target is assumed to be perfectly black viewed against the sky during daylight conditions.

With these assumptions it may then be shown (Ref. 6),

$$D_m = \frac{1}{\beta} \ln(1/.02). \tag{13}$$

It should be noted that observations of natural targets at various distances usually violate, at least to some extent, one or more of the assumptions, and provides only a crude approximation for the visual range and thus the aerosol number density required for the computations carried out here.

Aerosol number densities are often measured directly by a number of techniques, but without a collateral measurement of scattering cross section, and size distribution. These observations are of little use in the present study. The most relevant observations are of attenuation coefficient for desert locations. Two such references were found in a literature search.

Crosby and Koerber (Ref. 7) designed, built, and operated a nephelometer to automatically measure β at half hour intervals. Results from the operation of this instrument for about a year at Woomera, Australia are shown in Figure 1. Although β is expressed in terms of visual range by means of Equation 12, the measurements are not simply observations of a target, but rather actual measurements of the light scattered by aerosol particles into a sensitive and carefully calibrated photometer. The monthly mean of the observations is shown by the curve, the standard deviation by the heavy bars, and the range by the longer bars. The abscissa begins with data for July and ends with June data.

Spinhirne (Ref. 8) reports the mean and standard deviation of similar observations made by lidar techniques at Tuscon during the full winter and spring of 1975-76. These observations are indicated by the hashed region in Figure 1. These two sets of measurements seem to be consistent with each other and with qualitative observations that objects 35 to 70 miles away are often visible in the desert. We conclude that quantitative visual ranges in desert regions commonly range from 50 to 120km ($\sim$ 30 to 75 miles).

The aerosol number density and extinction coefficient, B, in the LOWTA/LOWTRAN3 program are normalized to 23km visual range (Refs. 4 and 5) through the work of Elterman (Ref. 9). From the preceding discussion, fractions of 1, .5, .25 and .1 of the number density for 23km visual range correspond to visual ranges of 23, 46, 92, and 230km, respectively. Four aerosol models with ground level number densities corresponding to these visual ranges were then created by smoothly joining these ground level number densities into a single standard LOWTRAN aerosol model at 5km altitude and above. The combination of these four aerosol models with three water-temperature-pressure profiles permits a possibility of 12 model atmospheres, all of which have been considered in this study.

IV. COMPUTATION RESULTS AND DISCUSSION

Calculations of I_p and I_0 (Equations 3 and 6) were made for incoming solar radiation at 0, 15, 30, 45, 60, and 70 degree zenith angles for each of the 12 model atmospheres. For most of these cases a tower 100m above the heliostat level was considered at a horizontal distance of h = 500, 250, or 125m from the base of the tower. The attenuation of these additional paths is expressed in terms of the direct energy as the fraction y in Tables 5 and 6 for a selected sample of cases.

Table 5 shows the percent reduction for various tower distances and water vapor models with a constant aerosol model corresponding to 23km visual range. Figure 2 summarizes the lack of dependence on water vapor model by plotting the reduction due to heliostat-tower path for a 30° solar zenith angle and 500m tower-heliostat distance. Figure 3, also drawn from the information of Table 5, illustrates two other features of the tower heliostat reduction. The reduction is approximately linearly dependent on tower-heliostat distance and largely independent of incoming solar zenith angle.

Table 6 shows the results of computations for the mid-latitude winter atmosphere and 500m tower-heliostat distance while the aerosol model is varied. The percent reduction due to the tower-heliostat path is shown and also the transmittance from space to the heliostat. These results are shown graphically for a 0° solar zenith angle in Figure 4.

A typical reduction of about two to four percent for the 500m tower-heliostat path can be obtained from Figure 4, recalling typical visual ranges in desert regions are 50 to 120km.

If the transmittance effects of the tower-heliostat path are assumed to be expressed in the form

$$T = \exp(-\gamma L), \qquad (14)$$

where L is the line of sight distance from the heliostat to the receiver then this study shows reasonable values of γ for desert locations are between 0.04 and .08km^{-1}. These values are consistent with a value of γ = .036km^{-1} used in modeling the atmospheric transmittance of the Nevada test site in the time period of the late 1950's and early 1960's (Ref. 10).

Table 1. Extraterrestrial Solar Irradiance Spectrum (Ref. 2)

λ(μm)	P_λ	D_λ	λ(μm)	P_λ	D_λ	λ(μm)	P_λ	D_λ
0.12	0.0000_1	0.00_+	0.43	0.1639	12.47	0.90	0.0889	63.36
0.14	0.0000_+	0.00_1	0.44	0.1810	13.73	1.00	0.0746	69.46
0.16	0.0000_2	0.00_1	0.45	0.2006	15.14	0.20	0.0484	78.39
0.18	0.0001	0.00_2	0.46	0.2066	16.65	0.40	0.0336	84.34
0.20	0.0011	0.01	0.47	0.2033	18.17	0.60	0.0244	88.61
0.22	0.0057	0.05	0.48	0.2074	19.68	0.80	0.0159	91.59
0.23	0.0067	0.10	0.49	0.1950	21.15	2.00	0.0103	93.49
0.24	0.0063	0.14	0.50	0.1942	22.60	0.20	0.0079	94.83
0.25	0.0070	0.19	0.51	0.1882	24.01	0.40	0.0064	95.89
0.26	0.0130	0.27	0.52	0.1833	25.38	0.60	0.0048	96.67
0.27	0.0232	0.41	0.53	0.1842	26.74	0.80	0.0039	97.31
0.28	0.0222	0.56	0.54	0.1783	28.08	3.00	0.0031	97.83
0.29	0.0482	0.81	0.55	0.1725	29.38	0.20	0.0023	98.22
0.30	0.0514	1.21	0.56	0.1695	30.65	0.40	0.0017	98.50
0.31	0.0689	1.65	0.57	0.1712	31.91	0.60	0.0013	98.72
0.32	0.0830	2.22	0.58	0.1715	33.18	0.80	0.0011	98.91
0.33	0.1059	2.93	0.59	0.1700	34.44	4.00	0.0009	99.06
0.34	0.1074	3.72	0.60	0.1666	35.68	4.50	0.0006	99.34
0.35	0.1093	4.52	0.62	0.1602	38.10	5.00	0.0004	99.51
0.36	0.1068	5.32	0.64	0.1544	40.42	6.00	0.0002	99.72
0.37	0.1181	6.15	0.66	0.1486	42.66	7.00	0.0001	99.82
0.38	0.1120	7.00	0.68	0.1427	44.81	8.00	0.0001	99.88
0.39	0.1098	7.82	0.70	0.1369	46.88	10.00	0.0000_3	99.94
0.40	0.1429	8.73	0.72	0.1314	48.86	15.00	0.0000.	99.98
0.41	0.1751	9.92	0.75	0.1235	51.69	20.00	0.0000.	99.99
0.42	0.1747	11.22	0.80	0.1107	56.02	50.00	0.0000.	100.00

P_λ, Solar spectral irradiance averaged over small bandwidth centred at λ, in W cm^{-2} μm^{-1}; D_λ, percentage of the solar constant associated with wavelengths shorter than λ.

Table 2. Solar Irradiance at Evenly Spaced Intervals of Frequency

	Frequency (cm^{-1})	Irradiance ($W\ m^{-2}\ \mu m^{-1}$)		Frequency (cm^{-1})	Irradiance ($W\ m^{-2}\ \mu m^{-1}$)		Frequency (cm^{-1})	Irradiance ($W\ m^{-2}\ \mu m^{-1}$)
1	.20000000E+04	.38300000E+01	57	.16000000E+05	.15900000E+04	114	.30250000E+05	.10600000E+04
2	.22500000E+04	.62500000E+01	58	.16250000E+05	.16200000E+04	115	.30500000E+05	.10300000E+04
3	.25000000E+04	.95000000E+01	59	.16500000E+05	.16500000E+04	116	.30750000E+05	.98500000E+03
4	.27500000E+04	.13000000E+02	60	.16750000E+05	.16700000E+04	117	.31000000E+05	.88500000E+03
5	.30000000E+04	.18300000E+02	61	.17000000E+05	.17000000E+04	118	.31250000E+05	.83000000E+03
6	.32500000E+04	.27000000E+02	62	.17250000E+05	.17160000E+04	119	.31500000E+05	.73500000E+03
7	.35000000E+04	.36800000E+02	63	.17500000E+05	.17200000E+04	120	.31750000E+05	.76500000E+03
8	.37500000E+04	.44800000E+02	64	.17750000E+05	.17000000E+04	121	.32000000E+05	.73000000E+03
9	.40000000E+04	.55000000E+02	65	.18000000E+05	.17200000E+04	122	.32250000E+05	.69000000E+03
10	.42500000E+04	.65500000E+02	66	.18250000E+05	.17300000E+04	123	.32500000E+05	.65500000E+03
11	.45000000E+04	.76500000E+02	67	.18500000E+05	.17800000E+04	124	.32750000E+05	.61000000E+03
12	.47500000E+04	.89500000E+02	68	.18750000E+05	.18200000E+04	125	.33000000E+05	.55000000E+03
13	.50000000E+04	.10300000E+03	69	.19000000E+05	.18500000E+04	126	.33250000E+05	.51800000E+03
14	.52500000E+04	.12400000E+03	70	.19250000E+05	.18300000E+04	127	.33500000E+05	.53000000E+03
15	.55000000E+04	.15300000E+03	71	.19500000E+05	.18700000E+04	128	.33750000E+05	.57500000E+03
16	.57500000E+04	.18300000E+03	72	.19750000E+05	.19200000E+04	129	.34000000E+05	.57500000E+03
17	.60000000E+04	.21700000E+03	73	.20000000E+05	.19420000E+04	130	.34250000E+05	.51000000E+03
18	.62500000E+04	.24500000E+03	74	.20250000E+05	.19700000E+04	131	.34500000E+05	.48000000E+03
19	.65000000E+04	.27000000E+03	75	.20500000E+05	.19500000E+04	132	.34750000E+05	.39500000E+03
20	.67500000E+04	.29700000E+03	76	.20750000E+05	.20400000E+04	133	.35000000E+05	.33000000E+03
21	.70000000E+04	.32200000E+03	77	.21000000E+05	.20600000E+04	134	.35250000E+05	.27500000E+03
22	.72500000E+04	.34600000E+03	78	.21250000E+05	.20400000E+04	135	.35500000E+05	.24200000E+03
23	.75000000E+04	.36800000E+03	79	.21500000E+05	.20400000E+04	136	.35750000E+05	.22200000E+03
24	.77500000E+04	.40000000E+03	80	.21750000E+05	.20660000E+04	137	.36000000E+05	.21200000E+03
25	.80000000E+04	.43800000E+03	81	.22000000E+05	.20500000E+04	138	.36250000E+05	.20400000E+03
26	.82500000E+04	.47300000E+03	82	.22250000E+05	.20000000E+04	139	.36500000E+05	.20500000E+03
27	.85000000E+04	.50800000E+03	83	.22500000E+05	.18900000E+04	140	.36750000E+05	.21500000E+03
28	.87500000E+04	.54500000E+03	84	.22750000E+05	.18000000E+04	141	.37000000E+05	.22800000E+03
29	.90000000E+04	.58100000E+03	85	.23000000E+05	.16500000E+04			
30	.92500000E+04	.61900000E+03	86	.23250000E+05	.16300000E+04			
31	.95000000E+04	.66100000E+03	87	.23500000E+05	.16900000E+04			
32	.97500000E+04	.70500000E+03	88	.23750000E+05	.17300000E+04			
33	.10000000E+05	.74800000E+03	89	.24000000E+05	.17700000E+04			
34	.10250000E+05	.79500000E+03	90	.24250000E+05	.17800000E+04			
35	.10500000E+05	.83500000E+03	91	.24500000E+05	.17200000E+04			
36	.10750000E+05	.85000000E+03	92	.24750000E+05	.16000000E+04			
37	.11000000E+05	.88300000E+03	93	.25000000E+05	.14290000E+04			
38	.11250000E+05	.90500000E+03	94	.25250000E+05	.12200000E+04			
39	.11500000E+05	.95000000E+03	95	.25500000E+05	.11200000E+04			
40	.11750000E+05	.99000000E+03	96	.25750000E+05	.10900000E+04			
41	.12000000E+05	.10300000E+04	97	.26000000E+05	.11000000E+04			
42	.12250000E+05	.10700000E+04	98	.26250000E+05	.11100000E+04			
43	.12500000E+05	.11090000E+04	99	.26500000E+05	.11300000E+04			
44	.12750000E+05	.11400000E+04	100	.26750000E+05	.11600000E+04			
45	.13000000E+05	.11800000E+04	101	.27000000E+05	.11800000E+04			
46	.13250000E+05	.12200000E+04	102	.27250000E+05	.11500000E+04			
47	.13500000E+05	.12600000E+04	103	.27500000E+05	.11100000E+04			
48	.13750000E+05	.13000000E+04	104	.27750000E+05	.10700000E+04			
49	.14000000E+05	.13400000E+04	105	.28000000E+05	.10700000E+04			
50	.14250000E+05	.13600000E+04	106	.28250000E+05	.10900000E+04			
51	.14500000E+05	.14100000E+04	107	.28500000E+05	.10900000E+04			
52	.14750000E+05	.14300000E+04	108	.28750000E+05	.10800000E+04			
53	.15000000E+05	.14700000E+04	109	.29000000E+05	.10650000E+04			
54	.15250000E+05	.14950000E+04	110	.29250000E+05	.10700000E+04			
55	.15500000E+05	.15300000E+04	111	.29500000E+05	.10750000E+04			
56	.15750000E+05	.15600000E+04	112	.29750000E+05	.10800000E+04			
			113	.30000000E+05	.10700000E+04			

Table 3. Relative Transmittance R of Pyrex Glass

	Frequency (cm^{-1})	Response		Frequency (cm^{-1})	Response		Frequency (cm^{-1})	Response
1	.20000000E+04	0.	58	.16250000E+05	.91000000E+00	115	.30500000E+05	.79000000E+00
2	.22500000E+04	.18000000E+00	59	.16500000E+05	.91000000E+00	116	.30750000E+05	.77000000E+00
3	.25000000E+04	.20000000E+00	60	.16750000E+05	.90500000E+00	117	.31000000E+05	.75000000E+00
4	.27500000E+04	.32000000E+00	61	.17000000E+05	.90500000E+00	118	.31250000E+05	.71000000E+00
5	.30000000E+04	.53000000E+00	62	.17250000E+05	.90500000E+00	119	.31500000E+05	.68000000E+00
6	.32500000E+04	.58000000E+00	63	.17500000E+05	.90500000E+00	120	.31750000E+05	.64000000E+00
7	.35000000E+04	.56000000E+00	64	.17750000E+05	.90500000E+00	121	.32000000E+05	.59000000E+00
8	.37500000E+04	.70000000E+00	65	.18000000E+05	.90500000E+00	122	.32250000E+05	.55000000E+00
9	.40000000E+04	.79000000E+00	66	.18250000E+05	.90500000E+00	123	.32500000E+05	.49000000E+00
10	.42500000E+04	.85000000E+00	67	.18500000E+05	.90500000E+00	124	.32750000E+05	.44000000E+00
11	.45000000E+04	.87000000E+00	68	.18750000E+05	.90500000E+00	125	.33000000E+05	.39000000E+00
12	.47500000E+04	.90000000E+00	69	.19000000E+05	.90500000E+00	126	.33250000E+05	.33000000E+00
13	.50000000E+04	.90500000E+00	70	.19250000E+05	.90500000E+00	127	.33500000E+05	.31000000E+00
14	.52500000E+04	.91000000E+00	71	.19500000E+05	.90500000E+00	128	.33750000E+05	.28000000E+00
15	.55000000E+04	.91000000E+00	72	.19750000E+05	.90500000E+00	129	.34000000E+05	.23000000E+00
16	.57500000E+04	.91000000E+00	73	.20000000E+05	.90500000E+00	130	.34250000E+05	.19000000E+00
17	.60000000E+04	.91000000E+00	74	.20250000E+05	.90500000E+00	131	.34500000E+05	.15000000E+00
18	.62500000E+04	.91000000E+00	75	.20500000E+05	.90500000E+00	132	.34750000E+05	.12000000E+00
19	.65000000E+04	.91000000E+00	76	.20750000E+05	.90500000E+00	133	.35000000E+05	.90000000E-01
20	.67500000E+04	.91000000E+00	77	.21000000E+05	.90000000E+00	134	.35250000E+05	.70000000E-01
21	.70000000E+04	.91000000E+00	78	.21250000E+05	.90000000E+00	135	.35500000E+05	.50000000E-01
22	.72500000E+04	.91000000E+00	79	.21500000E+05	.90000000E+00	136	.35750000E+05	.35000000E-01
23	.75000000E+04	.91000000E+00	80	.21750000E+05	.90000000E+00	137	.36000000E+05	.30000000E-01
24	.77500000E+04	.91000000E+00	81	.22000000E+05	.90000000E+00	138	.36250000E+05	.20000000E-01
25	.80000000E+04	.91000000E+00	82	.22250000E+05	.90000000E+00	139	.36500000E+05	.10000000E-01
26	.82500000E+04	.91000000E+00	83	.22500000E+05	.90000000E+00	140	.36750000E+05	0.
27	.85000000E+04	.91000000E+00	84	.22750000E+05	.90000000E+00	141	.37000000E+05	0.
28	.87500000E+04	.91000000E+00	85	.23000000E+05	.90000000E+00			
29	.90000000E+04	.91000000E+00	86	.23250000E+05	.90000000E+00			
30	.92500000E+04	.91000000E+00	87	.23500000E+05	.90000000E+00			
31	.95000000E+04	.91000000E+00	88	.23750000E+05	.90000000E+00			
32	.97500000E+04	.91000000E+00	89	.24000000E+05	.90000000E+00			
33	.10000000E+05	.91000000E+00	90	.24250000E+05	.90000000E+00			
34	.10250000E+05	.91000000E+00	91	.24500000E+05	.90000000E+00			
35	.10500000E+05	.91000000E+00	92	.24750000E+05	.90000000E+00			
36	.10750000E+05	.91000000E+00	93	.25000000E+05	.90000000E+00			
37	.11000000E+05	.91000000E+00	94	.25250000E+05	.90000000E+00			
38	.11250000E+05	.91000000E+00	95	.25500000E+05	.90000000E+00			
39	.11500000E+05	.91000000E+00	96	.25750000E+05	.90000000E+00			
40	.11750000E+05	.91000000E+00	97	.26000000E+05	.90000000E+00			
41	.12000000E+05	.91000000E+00	98	.26250000E+05	.90000000E+00			
42	.12250000E+05	.91000000E+00	99	.26500000E+05	.90000000E+00			
43	.12500000E+05	.91000000E+00	100	.26750000E+05	.90000000E+00			
44	.12750000E+05	.91000000E+00	101	.27000000E+05	.90000000E+00			
45	.13000000E+05	.91000000E+00	102	.27250000E+05	.90000000E+00			
46	.13250000E+05	.91000000E+00	103	.27500000E+05	.90000000E+00			
47	.13500000E+05	.91000000E+00	104	.27750000E+05	.89500000E+00			
48	.13750000E+05	.91000000E+00	105	.28000000E+05	.89000000E+00			
49	.14000000E+05	.91000000E+00	106	.28250000E+05	.88500000E+00			
50	.14250000E+05	.91000000E+00	107	.28500000E+05	.88000000E+00			
51	.14500000E+05	.91000000E+00	108	.28750000E+05	.87000000E+00			
52	.14750000E+05	.91000000E+00	109	.29000000E+05	.86000000E+00			
53	.15000000E+05	.91000000E+00	110	.29250000E+05	.84500000E+00			
54	.15250000E+05	.91000000E+00	111	.29500000E+05	.84000000E+00			
55	.15500000E+05	.91000000E+00	112	.29750000E+05	.83500000E+00			
56	.15750000E+05	.91000000E+00	113	.30000000E+05	.82500000E+00			
57	.16000000E+05	.91000000E+00	114	.30250000E+05	.81000000E+00			

Table 4. Normalized Pyrex and Solar Irradiance Function, r(ν)

FREQUENCY (CM-1)	TRANS.	FREQUENCY (CM-1)	TRANS.	FREQUENCY (CM-1)	TRANS.	FREQUENCY (CM-1)	TRANS.
2000.000	0.000000	2250.000	.032240	2500.000	.044110	2750.000	.079810
3000.000	.156400	3250.000	.215100	3500.000	.244100	3750.000	.323600
4000.000	.394000	4250.000	.447200	4500.000	.476900	4750.000	.518000
5000.000	.541100	5250.000	.594000	5500.000	.667800	5750.000	.730800
6000.000	.795900	6250.000	.828100	6500.000	.843800	6750.000	.860700
7000.000	.867700	7250.000	.869100	7500.000	.863600	7750.000	.879300
8000.000	.903600	8250.000	.917600	8500.000	.928400	8750.000	.939900
9000.000	.947100	9250.000	.955200	9500.000	.967000	9750.000	.979200
10000.000	.987600	10250.000	.999100	10500.000	1.000000	10750.000	.971200
11000.000	.960300	11250.000	.944100	11500.000	.948500	11750.000	.946800
12000.000	.944400	12250.000	.941500	12500.000	.937100	12750.000	.925900
13000.000	.921900	13250.000	.917500	13500.000	.912800	13750.000	.907900
14000.000	.902700	14250.000	.884300	14500.000	.885500	14750.000	.867800
15000.000	.862600	15250.000	.848800	15500.000	.840900	15750.000	.830300
16000.000	.820100	16250.000	.810000	16500.000	.800200	16750.000	.781600
17000.000	.772400	17250.000	.757200	17500.000	.737500	17750.000	.708500
18000.000	.697100	18250.000	.682100	18500.000	.682900	18750.000	.679800
19000.000	.672900	19250.000	.648500	19500.000	.645800	19750.000	.646300
20000.000	.637500	20250.000	.630800	20500.000	.609300	20750.000	.622100
21000.000	.610000	21250.000	.589900	21500.000	.576300	21750.000	.570300
22000.000	.553100	22250.000	.527500	22500.000	.487500	22750.000	.454200
23000.000	.407300	23250.000	.393800	23500.000	.399600	23750.000	.400500
24000.000	.401300	24250.000	.395300	24500.000	.374200	24750.000	.341100
25000.000	.298600	25250.000	.249900	25500.000	.224900	25750.000	.214700
26000.000	.212500	26250.000	.210400	26500.000	.210100	26750.000	.211700
27000.000	.211400	27250.000	.202200	27500.000	.191700	27750.000	.180400
28000.000	.176200	28250.000	.175400	28500.000	.171300	28750.000	.164900
29000.000	.158000	29250.000	.153300	29500.000	.150600	29750.000	.147800
30000.000	.142300	30250.000	.136100	30500.000	.126900	30750.000	.116400
31000.000	.100200	31250.000	.087560	31500.000	.079050	31750.000	.070380
32000.000	.061030	32250.000	.052940	32500.000	.044090	32750.000	.036310
33000.000	.029580	33250.000	.022430	33500.000	.021240	33750.000	.020510
34000.000	.016600	34250.000	.011990	34500.000	.008777	34750.000	.005695
35000.000	.003518	35250.000	.002248	35500.000	.001393	35750.000	.000882
36000.000	.000712	36250.000	.000451	36500.000	.000223	36750.000	.000000
37000.000	0.000000						

Table 5. Percent Reduction of Solar Radiation by Heliostat-Tower Atmospheric Path for Various Model Atmospheres and 23km Visibility Aerosol Model

Solar Zenith Angle (Degrees)	Percent Reduction from Clear Vertical Winter Conditions	Additional Percent Reduction, y, Due to Heliostat-Tower Path, h		
		h = 125m	h = 250m	h = 500m
Mid-latitude Winter				
0	0.00	2.29	3.88	7.14
15	1.10	2.28	3.86	7.10
30	4.67	2.24	3.81	6.98
45	11.75	2.18	3.70	6.81
60	25.12	2.08	3.51	6.48
70	40.87	1.91	3.25	6.04
Mid-latitude Summer				
0	3.75	2.35	4.03	7.42
15	4.85	2.34	4.01	7.38
30	8.36	2.37	3.96	7.30
45	15.42	2.24	3.83	7.07
60	28.57	2.14	3.63	6.71
70	44.02	2.02	3.38	6.27
Tropical				
0	4.79	2.37	4.04	7.44
15	5.86	2.40	4.05	7.43
30	9.40	2.32	3.98	7.27
45	16.36	2.30	3.87	7.12
60	29.49	2.12	3.64	6.71
70	44.81	1.99	3.37	6.31

Table 6. Percent Reduction of Solar Radiation by Heliostat-Tower Atmospheric Path for Various Aerosol Models.
(All calculations are for mid-latitude winter model and 500m tower-heliostat distance. Transmittances are from space to heliostat.)

Visual Range (km)	Solar Zenith Angle					
	0 Degrees		45 Degrees		70 Degrees	
	Trans.	Reduc. y	Trans.	Reduc. y	Trans.	Reduc. y
23	64.4	7.08	58.6	6.81	39.3	6.04
46	70.2	4.30	63.3	4.01	45.5	3.52
92	72.2	2.78	65.8	2.56	49.0	2.15
230	73.5	1.85	67.4	1.65	51.5	1.34

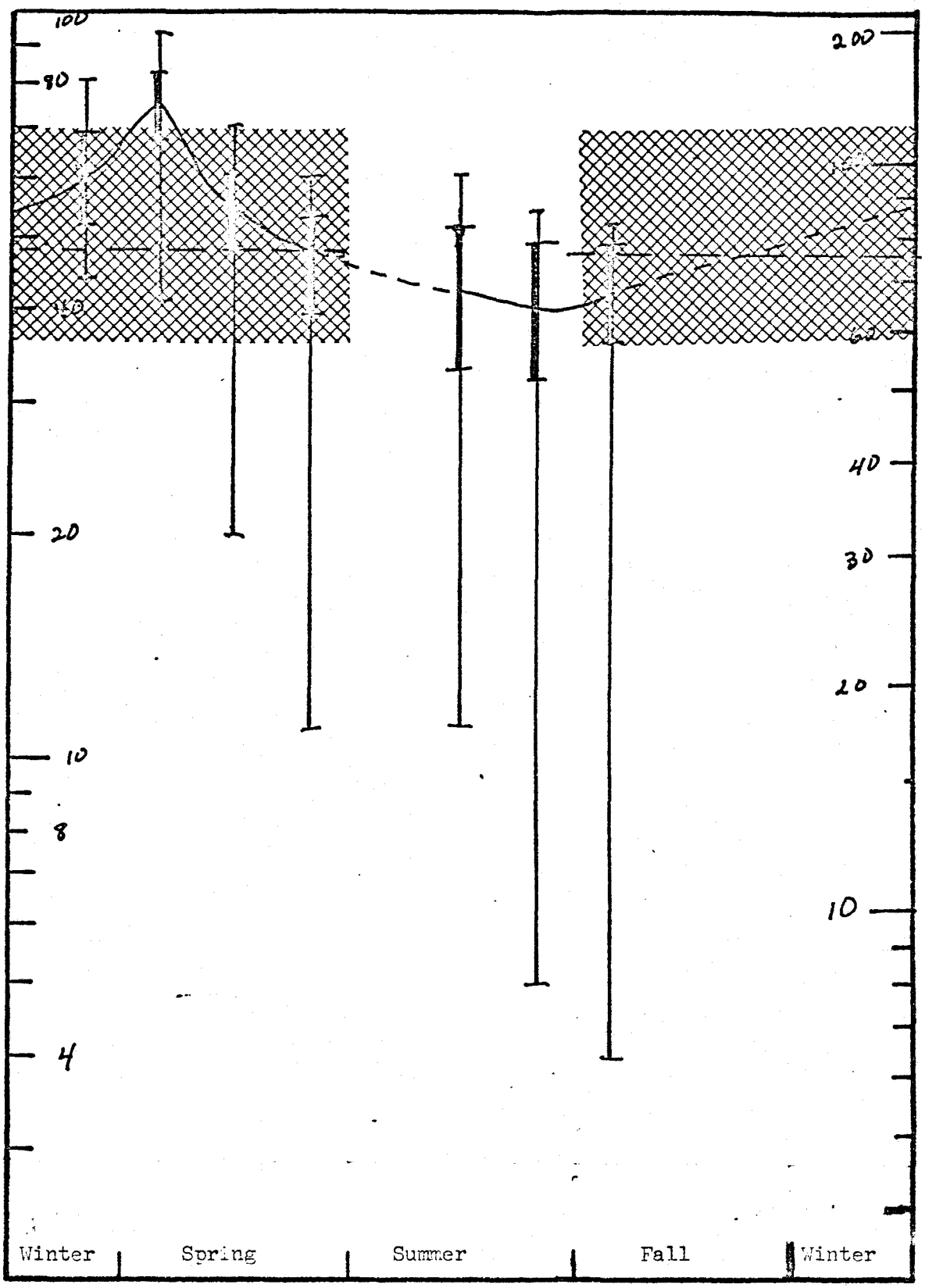

Figure 1. Observed aerosol attenuation coefficients, expressed as visual ranges, for Woomera Australia (Ref 7) and Tuscon Arizona (Ref 8). The curve connects monthly mean values from Woomera. The heavy bars are standard deviations and light bars are the range of monthly values from Woomera. The hashed area is the standard deviation of the values reported for Tuscon Arizona.

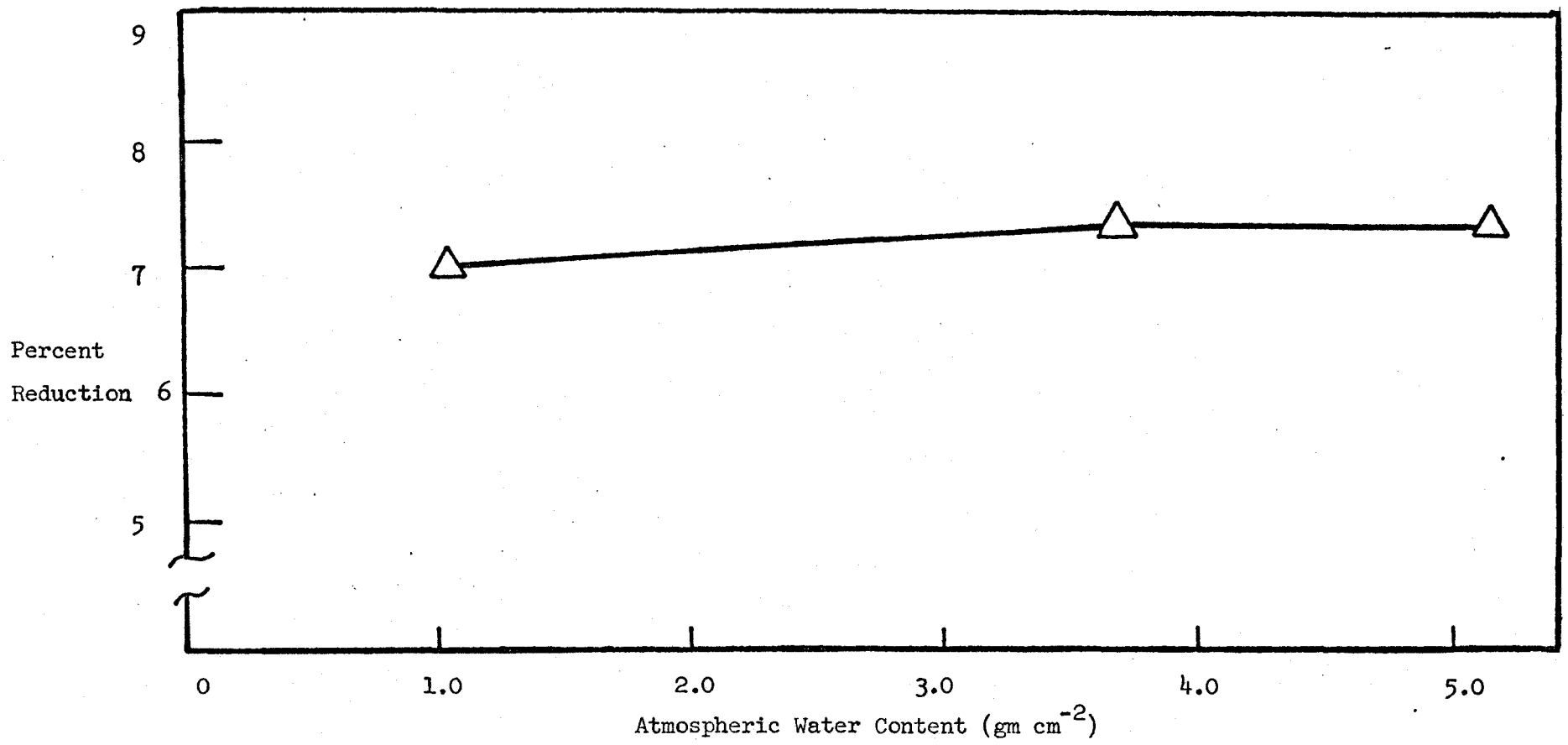

Figure 2. Percent reduction in radiation due to heliostat-tower path for various atmospheric water content models. All computations were made with a 30° solar zenith angle, a 23 km visual range aerosol model and a heliostat to tower base distance of 500 m.

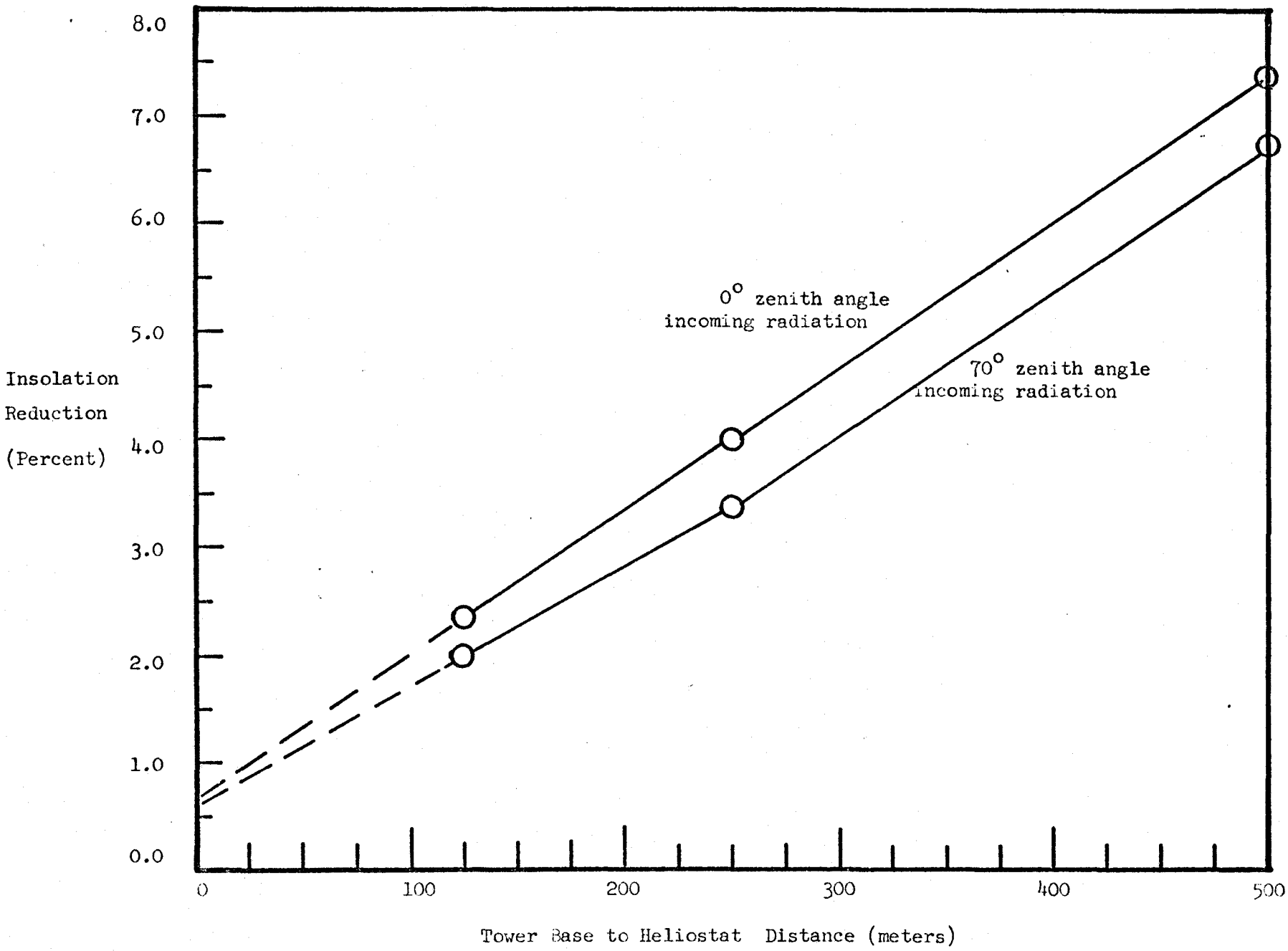

Figure 3. Reduction of insolation by atmospheric attenuation in the heliostat-tower path as a function of heliostat-tower distance for a midlattitude summer model atmosphere and 23 km visual range aerosol model.

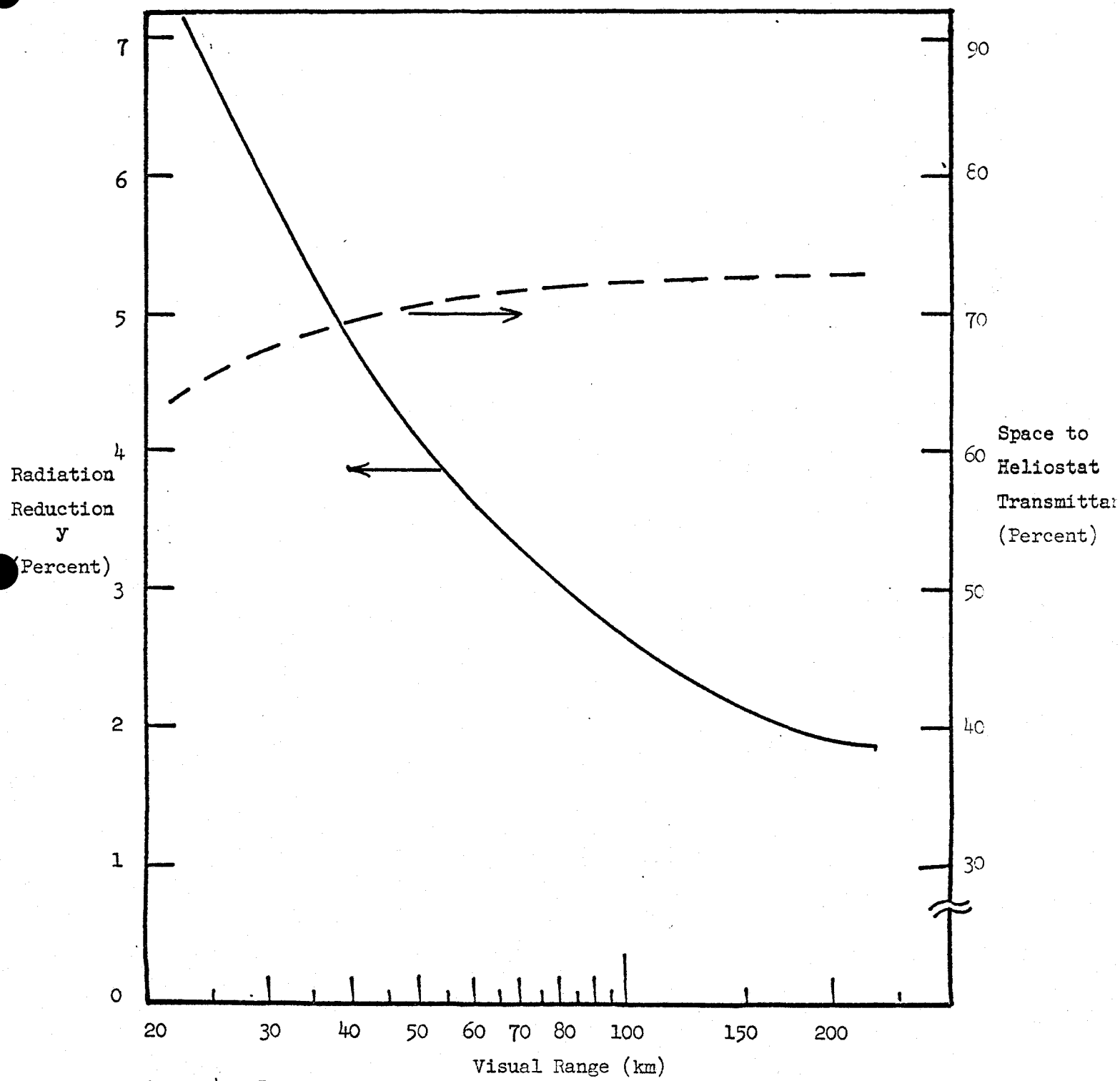

Figure 4. Percent reduction of radiation due to tower-heliostat path as a function of visual range.(Solid curve) The transmittance from space to the heliostat obtained as part of the same computation is also shown (dashed curve). All calculations were made for 0° solar zenith angle, midlatitude winter model atmosphere and 500 meter distance from tower base to heliostat

REFERENCES

1. C. M. Randall, "Relative Response of AlGaAs Photovoltaic Cells to Various Atmospheric Conditions", Aerospace Technical Memorandum ATM76(7574-02)-1, 25 March 1976.

2. M. P. Thekaekara and A. J. Drummond, "Standard Values for the Solar Constant and its Spectral Components," Nature Physical Science 229, 6 (1971).

3. C. M. Randall, "Low Resolution Transmittance Computer Program LOWTA User's Guide," Aerospace Technical Memorandum ATM75(5409-32)-6, 4 March 1975.

4. J. E. A. Selby and R. A. McClatchey, "Atmospheric Transmittance from 0.25 to 28.5μm: Computer Code LOWTRAN3." Air Force Cambridge Research Laboratories Environmental Research Paper 513, AFCRL-TR-75-0255, 7 May 1975.

5. R. A. McClatchey, et al., "Optical Properties of the Atmosphere (Third Edition)," Air Force Cambridge Research Laboratories Environmental Research Paper 411, AFCRL-72-0497, 24 August 1972.

6. F. A. Berry, E. Bolling, N. R. Beers, ed. "Handbook of Meteorology," McGraw Hill, Section III.

7. P. Crosby and B. W. Koerber, "Scattering of Light in the Lower Atmosphere," J. Opt. Soc. Am. 53, 358-361 (1963).

8. J. Spinhirne, "Monitoring of Tropospheric Aerosol Optical Properties by Lidar," Atmospheric Aerosols: Their Optical Properties and Effects NASA CP2004, Digest of Technical Papers presented at Williamsburg, Virginia, 13-15 December 1976.

9. L. Elterman, "Vertical-Attenuation Model with Eight Surface Meteorological Ranges 2 to 13 Kilometers," Air Force Geophysics Laboratory Environmental Research Paper 318, AFCRL-70-0200, March 1970.

10. J. R. Keith, P. B. Wells, M. E. Donaldson and E. A. Bathke, "Atmospheric Transmission of Nuclear Weapon Thermal Radiation." Kaman Sciences Corp., Report DNA-3223z, 9 September 1974.

ACKNOWLEDGMENT

The efficient assistance of M. E. Whitson, Jr. and S. S. Goldberg in searching the literature for relevant desert aerosol attenuation measurements is appreciated.